https://doi.org/10.5194/amt-2020-343
Preprint. Discussion started: 9 September 2020

Atmospheric Measurement Techniques Discussions

Prediction Model for Diffuser Induced Spectral Features in Imaging Spectrometers

Florian Richter[1,2], Corneli Keim[2], Jérôme Caron*, Jasper Krauser[2], Dennis Weise[2], and Mark Wenig[1]

[1]Meteorological Institute LMU Munich, Theresienstr. 37, Munich, Germany
[2]Airbus Defence and Space GmbH, Willy-Messerschmitt-Str. 1, 82024 Taufkirchen, Germany
*now at TNO, Optics Department, Stieltjesweg 1, 2628 CK Delft, The Netherlands

Correspondence: Florian Richter (flo.richter@physik.lmu.de)

Abstract. Wide-field spectrometers for Earth Observation missions require inflight radiometric calibration, for which the sun can be used as a known reference. Therefor a diffuser is placed in front of the spectrometer in order to scatter the incoming light into the entrance slit and provide homogeneous illumination. The diffuser however, introduces interference patterns known as speckles into the system, yielding potentially significant intensity variations at the detector plane, called Spectral Features.

There have been several approaches implemented to characterize the Spectral Features of a spectrometer, e.g. end-to-end measurements with representative instruments. Additionally, in previous publications a measurement technique was proposed, which is based on the acquisition of monochromatic speckles in the entrance slit following a numerical propagation through the disperser to the detection plane. Based on this measurement technique we present a standalone prediction model for the magnitude of Spectral Features in imaging spectrometers, requiring only few input parameters and therefor mitigating the need for expensive measurement campaigns.

1 Introduction

Many current and future Earth Observation missions carry wide field spectrometer payloads such as the ENVISAT Medium Resolution Imaging Spectrometer (Olij et al. (1997)), the Sentinel-2 MultiSpectral Imager (Martimort et al. (2012)), the Sentinel-3a Ocean and Land Colour Imager (Nieke and Mavrocordatos (2017)), the Sentinel-4 UVN instrument (Clermont et al. (2019)), the Sentinel-5-UVNS instrument (Guehne et al. (2017)), or the GHGIS instrument of CO2M or former CarbonSat (Fletcher et al. (2015)). These spaced based instruments require inflight radiometric calibration, for which the Sun can be used as a known reference. In order to ensure homogeneous illumination of the instrument a diffuser is used to scatter the incoming Sun light into the entrance slit. However, the diffuser introduces a statistical interference phenomenon known as speckles into the optical system. The speckles propagate through the disperser and are integrated at the detector plane, yielding intensity variations described as *Spectral Features* by van Brug et al. (2004). Since Spectral Features are of statistical nature and cannot be mitigated by any post-processing steps, they may pose a significant contributor to the radiometric error budget. In particular for spectrometers with fine spectral resolution and strict demands to radiometric accuracy it is important to determine the severity of this error in an instrument even in early planing phases. The magnitude of this error is commonly described in terms of the Spectral Features Amplitude (SFA) first introduced by van Brug and Courrèges-Lacoste (2007).

https://doi.org/10.5194/amt-2020-343
Preprint. Discussion started: 9 September 2020


Atmospheric Measurement Techniques Discussions

The issue of diffuser induced Spectral Features in imaging spectrometers has first been documented by Richter et al. (2002) and Wenig et al. (2004) in the context of the Global Ozone Monitoring Experiment (GOME). Ahlers et al. (2004) observed spectral oscillations caused by the onboard diffuser in the Scanning Imaging Absorption Spectrometer for Atmospheric Chartography (SCIAMACHY) instrument, as well as van Brug et al. (2004). Several approaches for characterization and modeling have been proposed since, e.g. end-to-end measurements by van Brug and Courrèges-Lacoste (2007) as well as models for different speckle averaging effects derived by van Brug and Scalia (2012). However, a comprehensive and reliable model has not been presented, yet. Isolating the Spectral Features by eliminating all other error sources in an representative end-to-end setup remains the main challenge to gain quantitative insights into the SFA dependence.

A different approach to quantify Spectral Features was taken by Burns et al. (2017) and improved by Richter et al. (2018). It is based on the subsequent acquisition of monochromatic speckle patterns in the slit plane over a certain wavelength range, which are then propagated numerically through the disperser to the detection plane. Some simplifying assumptions are made about the optical system which reduces the complexity and limits systematic error contributions. It is only limited by the SNR and the resolution achieved in the entrance slit and therefor capable of yielding comprehensive measurement data. Most important, it allows a step-by-step tracing of the speckle statistics from the slit to the detector plane.

Based on this SFA measurement technique we present a novel standalone SFA prediction model, which solely relies on mathematical descriptions of the speckle statistic and its SFA impact. It includes polarization effects of the diffuser, spatial and spectral averaging as well as pixel averaging at the detector.

First we review the definition of the Spectral Features Amplitude (SFA) in Sect. 2. In Sect. 3 the revised SFA measurement technique used for our measurements is shown. We then present the standalone SFA prediction model in Sect. 4, which can be understood as a mathematical formulation of the SFA measurement technique. Finally, we compare the results of the prediction model to our measurement chain in detail in Sect. 5 to show its validity. In the last section we dicuss the applicability to a real instrument.

2 Spectral Features Amplitude

The term *Spectral Features Amplitude* (SFA) was first proposed by van Brug and Courrèges-Lacoste (2007) as generic method to quantify diffuser induced "wiggles" in a spectrum measured by a space spectrometer instrument. They describe it as the magnitude of unwanted "features" that are left in the spectrum when subtracting all other features like emission lines from the source and atmospheric absorption. The SFA value is then calculated as the standard deviation of the normalized signal over a certain spectral width, that includes multiple features. The SFA value holds information about the amplitude of features. However, the data produced in this work, which is used to calculate the SFA, also allows for the estimation of the spectral extend of features. One usually may not draw conclusions about the absolute spectral positions of features with this approach. We will show that for high performance volume diffuser, such as the one used in this work, lead to a spectral extend smaller than the instrument detector pixel, which essentially allows for the treatment of the SFA as white noise at the detector level.

https://doi.org/10.5194/amt-2020-343
Preprint. Discussion started: 9 September 2020


Atmospheric Measurement Techniques Discussions

3 SFA Measurement Chain

In this Sect. the used SFA measurement technique introduced by Burns et al. (2017) is presented in a revised state. The goal of this technique is the reduction of experimental complexity and therefore systematic error contributions during data acquisition. First, the measurement principle is explained. Second, the used materials and the measurement procedures for the near infrared (NIR) and the short wavelength infrared (SWIR) channel are presented.

3.1 Principle

Figure 1 depicts the optical setup of an imaging spectrometer during solar calibration. The incoming Sun light is scattered by the diffuser. The scattering origin lies in the aperture plane with spatial coordinates g and h which is perpendicular to the light's direction of propagation. The angular field distribution at the aperture plane is imaged to the slit plane with coordinates x and y. The light is collimated onto a dispersive element (e.g a diffraction grating), which is splitting it into its spectral components. The spatial information in the y direction of the slit is transformed into spectral information at the detector with coordinate b by imaging the the diffracted beams of different wavelengths onto a 2D array detector. Beams of the same wavelength (within the spectral resolution) are assigned the same spectral detector coordinate b. The spatial information in x direction is retained in the detector coordinate a. We relate the coordinates via the simplified linear spectrometer equations

$$a = M_x x, \tag{1}$$

$$b = M_y y + k\lambda, \tag{2}$$

where M_x and M_y are the respective magnification factors in x and y direction, $k = db/d\lambda$ denotes the dispersion, and λ the wavelength. For these simplified equations to hold the magnification factors and the dispersion are assumed to be independent of the wavelength and the instrument point spread function (IPSF) is not accounted for. Additionally, a few properties of the Sun's light and its detection need to be considered. It is assumed to be spatially coherent giving the distance from the Sun to the Earth and the limited acceptance angle of the spectrometer. Additionally, the temporal coherence is very short compared to the detector integration time, which is in the order of seconds. It follows that cross coherence terms of interfering fields of different wavelengths vanish and the net intensity distributions at the slit and the detector planes are well approximated by the superposition of monochromatic intensities. The Sun disk comprises of many incoherent point sources, which should be considered for angular averaging contributions and is not part of this work, as it will only account for a single point source. For the purpose of the SFA measurement the sequence of optical components is subdivided into two parts. The first part ranging from the illuminated diffuser through the telescope to the entrance slit is represented by the optical setup in the lab. The second part comprises the rest of the optical system from the slit plane to the instrument detector plane. The data acquired in the first part is used as input for a numerical simulation of the optical setup after the slit plane. The setup layout is shown in Fig. 2. The Sun is mimicked as a single field point with a tunable laser source, which is spectrally stabilized by a wavemeter, and illuminates the diffuser through a linear polarizer at normal incident with respect to the diffuser plane. The distance between the single mode fiber output and the diffuser is chosen such that the divergent beam illuminates the diffuser homogeneously

https://doi.org/10.5194/amt-2020-343
Preprint. Discussion started: 9 September 2020

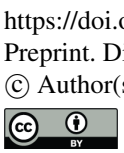

Atmospheric Measurement Techniques Discussions

over the size of the apertures. The second aperture blocks any unwanted angular contributions. A powermeter placed next to the diffuser records a fixed fraction of the emitted laser power. The telescope images the scattered light onto a 2D array detector positioned in the focal plane. The focal plane of the telescope represents the slit plane in Fig. 1. The diffuser plane is tilted by 10° with respect to aperture and slit plane. This ensures that only scattered light contributes to the measurement. The telescope is aligned perpendicular to the aperture and slit plane.

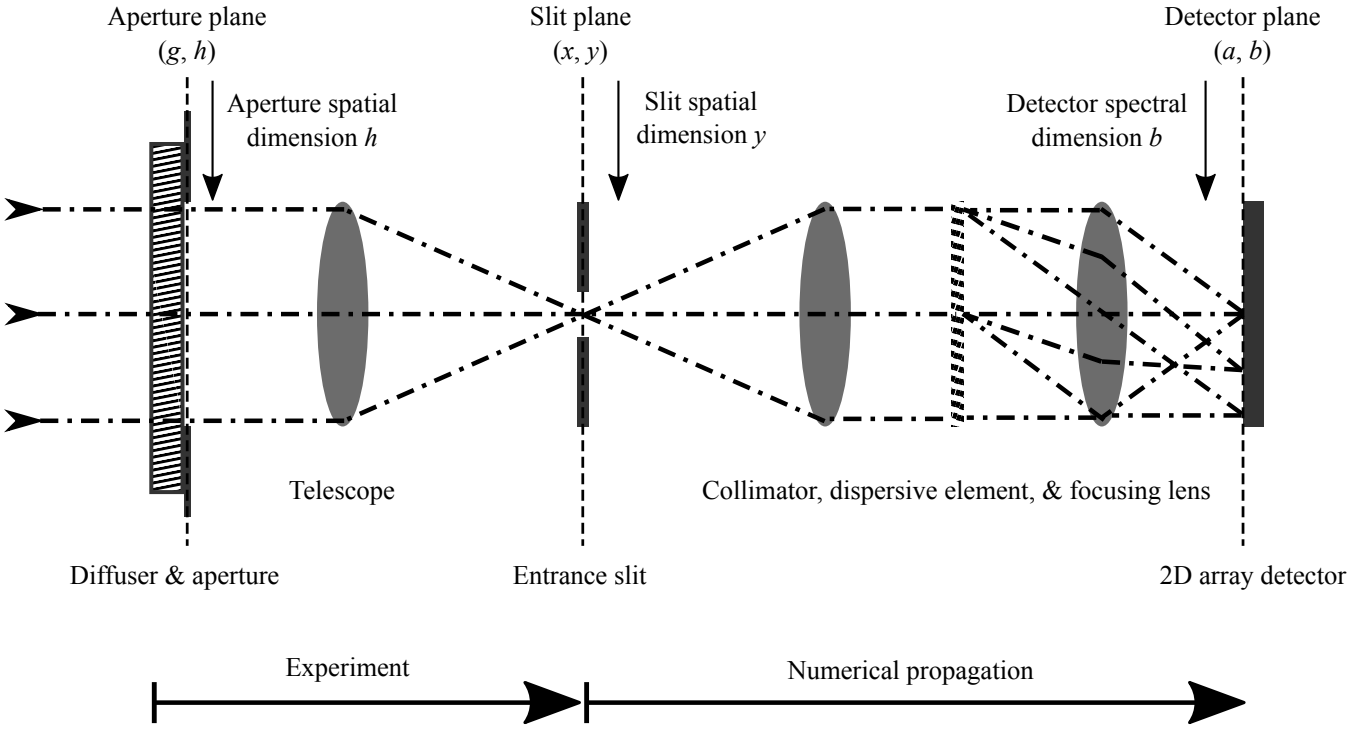

Figure 1. Optical setup of an imaging spectrometer during solar calibration. The sequence of optical components is subdivided into two parts. The first part is covered by the experimental setup in the lab starting at the illuminated diffuser and ending at the slit in the telescope focal plane. The second part numerically propagates the images recorded in the slit plane to the instrument focal plane.

For a measurement, monochromatic speckle intensities are recorded subsequently over a wavelength range $\lambda_1 ... \lambda_N$ several times the spectral resolution λ_{res} of the real spectrometer that is being mimicked. The spectral tuning step size $\Delta\lambda$ in between images needs to be sufficiently small, in order to properly sample the change of the speckle patterns. The intermediate result is a three dimensional data set $I_{slit}(x, y, \lambda)$ consisting of a spectrum of monochromatic speckle images, where x and y are the spatial coordinates in the slit plane and λ is the wavelength. Every speckle image is mapped to a certain position (a, b) at the focal plane, where all images are summed up in intensity. The summation on intensity basis is justified as cross coherence terms involving interference of different wavelengths of actual Sun light will vanish for sufficiently long integration times. The

https://doi.org/10.5194/amt-2020-343
Preprint. Discussion started: 9 September 2020

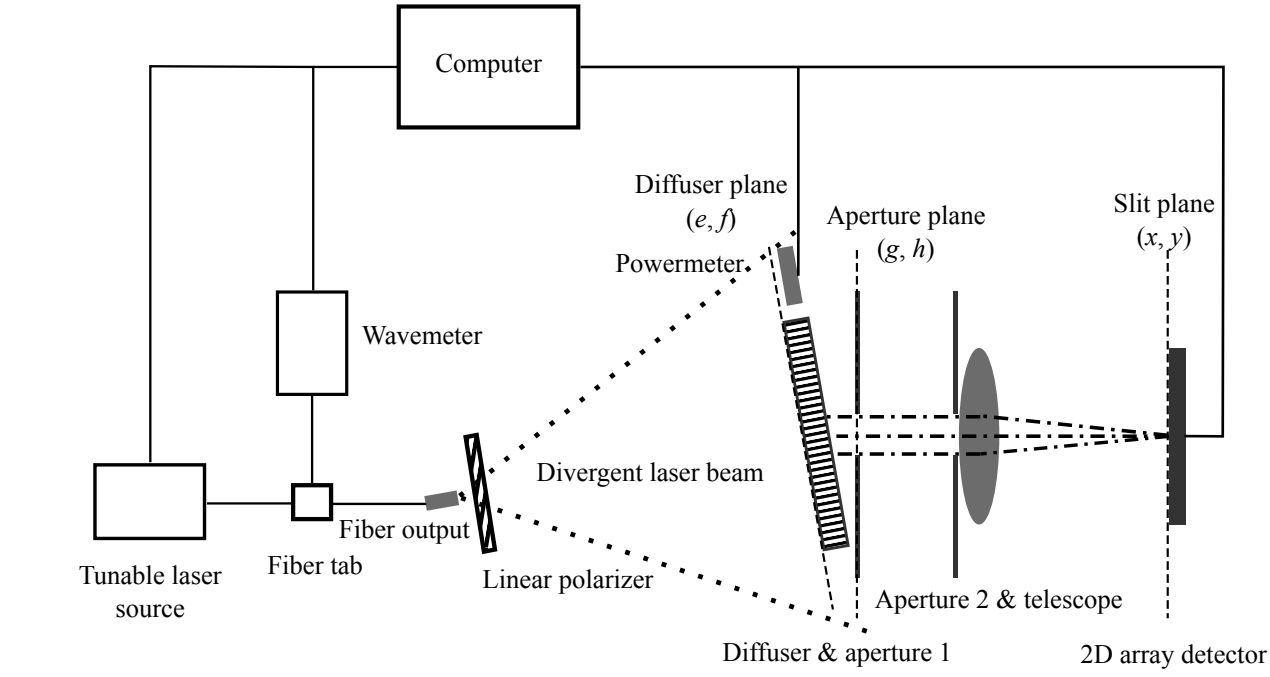

Figure 2. Layout of the experimental setup for measuring diffuser induced monochromatic speckle patterns in the slit plane.

summation procedure is detailed in Burns et al. (2017) and can be summarized as

$$I_{det}(a,b) = \frac{\Delta\lambda}{\lambda_{res}} \sum_{\lambda=\lambda_1}^{\lambda_N} I_{slit}\left(\frac{a}{M_x}, \frac{b-k\lambda}{M_y}, \lambda\right) \Theta\left(b-k\lambda\right), \tag{3}$$

where slit coordinates are expressed in terms of the detector coordinates using Eq. (1) and (2) and the Heavyside function with $\Theta(y) = 0, y < 0$ and $\Theta(y) = 1, y \geq 0$. The result of the sum is a two dimensional intensity distribution in the focal plane of the instrument $I_{det}(a,b)$. In a last step $I_{det}(a,b)$ is overlayed with the actual instruments detector pixel grid $(\tilde{a},\tilde{b})$and intensities belonging to the same pixel are summed. The SFA is calculated as standard deviation of the normalized detector pixel intensity distribution $I_{det,binned}(\tilde{a},\tilde{b})$.

3.2 Materials and Procedure

Measurements are conducted in the NIR regime around 777 nm and in the SWIR regime around 1570 nm which represent wavelength bands with commonly monitored data products, such as water, clouds, CO2, Aerosols, or the O2 absorption which is commonly used to calculate the effective path length and the air mass factor. The experimental setup is shown in Sect. 3.1. As light sources serve tunable monochromatic external cavity diode lasers with single mode output and an integrated optical isolator. They are stabilized via a proportional-integral-derivative (PID) loop with feedback data from a wavemeter, which uses a Fizeau interferometer. A linear polarizer ensures polarization stability. The round diffuser plate has a diameter of 70 mm and

https://doi.org/10.5194/amt-2020-343
Preprint. Discussion started: 9 September 2020


Atmospheric Measurement Techniques Discussions

a thickness of 3 mm. It is made of highly scattering fused silica HOD®-500 material. The data collected with the powermeter is used to normalize the acquired images. The round apertures are used to control the size of individual speckle correlation areas. The telescope has a focal length of $f_{tel} = 1100\text{mm}$. For the NIR the laser source has a center wavelength of 780 nm and a nominal linewidth of 300 kHz. The CCD detector features a 12.5 mm x 10.0 mm active area with 2750 x 2200 pixels of size 4.54 µm x 4.54 µm. The expected speckle size S_d in the slit plane is calculated using

$$S_d = \frac{\lambda f_{tel}}{D/2\sqrt{\pi}}, \tag{4}$$

where S_d is the width of the aperture function in the slit plane. Thus a single speckle is sampled by 14 pixel in one dimension, which is deemed sufficiently fine to ensure that the sampling with the detector does not alter the speckle pattern significantly. The laser wavelength was tuned over the range of 776.0 nm-777.8 nm with a step size of $\Delta\lambda = 1\text{pm}$. The step size is chosen, so that there is a non zero correlation between subsequent speckle images. For the SWIR measurement the laser source as well as the detector and the fiber splitter are replaced. The SWIR laser source center wavelength is 1550 nm, with single mode output of nominal 150 kHz linewidth. The detector is a 640 x 512 pixel InGaAs camera with a pixel size of 15.5 μm x 15.5 μm. The tuning range was 1570nm-1573nm with a step size of $\Delta\lambda = 2.5\text{pm}$. The apertures' diameter is set to $D = 10\text{mm}$ yielding an estimated expected speckle oversampling ratio of 13.

4 Spectral Features Amplitude Prediction Model

The prediction model presented in the following is a mathematical formulation of the measurement method described in Sect. 3. It relies on the determination of the speckle statistics at different steps of the measurement chain. The relevant physical information about speckle averaging effects in the measurement chain lies in the intensity distributions. A single pattern I is sampled by a finite but sufficient amount of pixel, so that the individual pixel size is small compared to the speckle size. The magnitude of the speckle effect in I is described as the *speckle contrast* (Goodman, 2007, p. 28)

$$C = \frac{\sigma_I}{\langle I \rangle}, \tag{5}$$

where σ_I is the standard deviation and $\langle I \rangle$ is the mean value of I over all pixel. Under the general assumption, that the individual statistics of the underlying fields are circular complex Gaussian, a fully developed speckle pattern generated with linear polarized monochromatic light has a contrast of $C = 1$ (Goodman, 2007, p. 29). We adopt this assumption for this model. The speckle contrast is reduced by several averaging effects introduced by the spectrometer instrument. A reduction of C is only achieved by the summation of intensity distributions showing a correlation smaller than unity. If the summation is on amplitude basis (when the distributions can interfere), C is not reduced (Goodman, 2007, section 3.1.1). From this follows, that only distributions which can not interfere will impact C and are therefore subject of further discussions. Each one of the N independent averaging effects attributes to a certain amount of *degrees of freedom* M_n or effectively uncorrelated intensity

https://doi.org/10.5194/amt-2020-343
Preprint. Discussion started: 9 September 2020


Atmospheric Measurement Techniques Discussions

distributions, which can be combined to a total averaging factor M according to (Goodman, 2007, p. 186) by

$$M = \prod_{n}^{N} M_n. \tag{6}$$

The reduced speckle contrast will then calculate to

$$C_{reduced} = \frac{1}{\sqrt{M}} = \left(\sqrt{\prod_{n}^{N} M_n} \right)^{-1}. \tag{7}$$

In order to predict the contrast reduction we identified $N = 3$ contributors, which can be assigned to different steps of the SFA measurement chain:

1. Generation of monochromatic diffuse depolarized light in the aperture plane (g, h),
2. mapping intensities in the slit plane (x, y) to instrument detector positions (a, b),
3. integration of the instrument detector pixels.

4.1 Polarization Averaging

The laser source emits a single polarization state, which is ensured with the polarizer. The diffuse light leaving the volume diffuser can be treated as depolarized due to multi scattering (Lorenzo, 2012, p.85). This corresponds to two orthogonal polarization configurations or two effective intensity distributions which can not interfere. Therefore step $n = 1$ introduces two degrees of freedom $M_{polarization} = 2$ (Goodman, 2007, p. 49).

4.2 Spectral Averaging

Step $n = 2$ leads to spectral averaging at the detector. We recall the finding from Sect. 3.1, that the net intensities in the field planes (slit and detector) can be treated as superposition of monochromatic intensities for integration times greater than the coherence time. Let us consider the acquired speckle intensities $I_n(x, y)$ and the underlying fields $A_n(x, y)$, which are related by $I_n = |A_n|^2$. They are recorded at frequencies $f_n = \frac{c}{\lambda_n}$ with a difference $\Delta f = f_m - f_n$ and c being the speed of light. The magnitude of the statistical change of subsequent speckle intensities I_m and I_n can be described in terms of the first order field correlation coefficient μ_{mn}, with

$$\mu_{mn}(\Delta f) = \frac{\langle A_m A_n^* \rangle}{\sqrt{\langle I_m \rangle \langle I_n \rangle}}. \tag{8}$$

The field correlation is influenced by two effects, which in our case are both frequency dependent. The first effect is due to changing light paths through the diffuser medium. The second effect takes into account the spatial offset $\Delta b = k \frac{c}{\Delta f}$ at the detector plane between individual speckle patterns I_n induced by the dispersion (see Eq. (2)). We start with the former contribution to the field correlation and follow the approach of Thompson et al. (1997a, b) and Webster et al. (2003), who

https://doi.org/10.5194/amt-2020-343
Preprint. Discussion started: 9 September 2020

Atmospheric Measurement Techniques Discussions

used an analytic diffusion model to describe the light propagation in highly scattering, non-absorbing diffusers. The diffusion model yields the path length probability density function $p(l)$ depending on the properties of the diffuser material, namely the scattering mean free path length l_s, the refractive index of the material n_s, and the thickness d. The characteristic function $F_l(\Delta f)$ is the frequency dependent representation of $p_l(l)$ and is given by

$$F_l(\Delta f) = \int_0^\infty p_l(l) \exp\left(\frac{i2\pi(1-n_s)\Delta f \alpha}{c} l\right) dl, \tag{9}$$

where c denotes the speed of light and α a constant factor taking into account the contribution of the tilted diffuser plane (e, f) with respect to the other planes and the specific geometry. The second contribution to the field correlation is due to changing spatial positions of speckle patterns which are distributed over the instrument detector in accordance with the spectral dispersion. This constitutes a spatial offset $\Delta b(\Delta f))$ between the speckle intensities I_n at the detector plane (a, b).The correlation of speckle fields, which are separated spatially by Δb can be expressed as

$$\Psi(\Delta b) = \frac{\int_\infty^\infty |P(h)|^2 e^{-i\frac{2\pi}{\tilde{\lambda}z} h \Delta b} dh}{\int_\infty^\infty |P(h)|^2 dh}, \tag{10}$$

where $P(h)$ is the aperture function of the imaging system, h is the y-coordinate representation in the aperture plane, z is the distance between pupil and image plane, and $\tilde{\lambda}$ the mean wavelength (Goodman, 2007, p. 169). Combining the two frequency dependent effects we can model the correlation between the speckle fields as

$$\mu_{mn}(\Delta f) = F_l(\Delta f)\Psi(\Delta b(\Delta f)). \tag{11}$$

The accumulation of individual speckle patterns I_n with field correlations μ_{mn} at the detector can be interpreted as the summation of partially correlated speckle intensities

$$I_{det}(a, b) = \sum_{n=1}^{N=\lambda_{res}/\Delta\lambda} I_n\left(\frac{a}{M_x}, \frac{b - k\lambda}{M_y}, \frac{c}{\lambda_n}\right). \tag{12}$$

The amount of individual speckle intensities I_n contributing to the sum at arbitrary detector coordinates (a, b) is equal to the ratio of the spectral resolution λ_{res} with the step size $\Delta\lambda$. This also applies to the mean intensities,

$$\langle I_{det}(a, b)\rangle = \sum_{n=1}^{N=\lambda_{res}/\Delta\lambda} \langle I_n\left(\frac{a}{M_x}, \frac{b - k\lambda}{M_y}, \frac{c}{\lambda_n}\right)\rangle. \tag{13}$$

Using an established method shown by Bevan (2009) and Goodman (2007) we define a coherency matrix with entries $J_{nm} = \langle A_m A_n^*\rangle$ and use Eq. (8) to get

$$\underline{J} = \begin{bmatrix} \langle I_1\rangle & \sqrt{\langle I_1\rangle\langle I_2\rangle}\mu_{1,2} & \cdots & \sqrt{\langle I_1\rangle\langle I_N\rangle}\mu_{1,N} \\ \sqrt{\langle I_1\rangle\langle I_2\rangle}\mu_{1,2}^* & \langle I_2\rangle & \cdots & \sqrt{\langle I_2\rangle\langle I_N\rangle}\mu_{2,N} \\ \vdots & \vdots & \ddots & \vdots \\ \sqrt{\langle I_1\rangle\langle I_N\rangle}\mu_{1,N}^* & \sqrt{\langle I_2\rangle\langle I_N\rangle}\mu_{2,N}^* & \cdots & \langle I_N\rangle \end{bmatrix}. \tag{14}$$

https://doi.org/10.5194/amt-2020-343
Preprint. Discussion started: 9 September 2020

Atmospheric Measurement Techniques Discussions

By diagonalization of $\underline{J}$ with a unitary linear transformation $\underline{L_0}$, the ensemble of correlated speckle fields is transformed to a basis with no correlation between them.

$$\underline{J'} = \underline{L_0}\underline{J}\underline{L_0}^{\dagger} = \begin{bmatrix} \langle \tilde{I_1} \rangle & 0 & \cdots & 0 \\ 0 & \langle \tilde{I_2} \rangle & \cdots & 0 \\ \vdots & \vdots & \ddots & \vdots \\ 0 & 0 & \cdots & \langle \tilde{I_N} \rangle \end{bmatrix}, \tag{15}$$

where † denotes the Hermitian transpose operation. The total mean intensity $\langle I_{det} \rangle = \sum_n \langle I_n \rangle = \sum_n \langle \tilde{I_n} \rangle$ is conserved under this transformation but in general $\langle I_n \rangle \neq \langle \tilde{I_n} \rangle$. The complex coherence factor $\mu_{mn} = |\mu_{mn}| \exp(i\Phi_{nm})$ includes a phase Φ_{nm}. However, due to the specific construction of $\underline{J}$, these phase terms can be omitted when calculating the eigenvalues (Dainty et al., 1975, section 4.7.2). Finally, for the spectral degrees of freedom we use the eigenvalues $\langle \tilde{I_n} \rangle$ of the coherency matrix to get

$$M_{spectral} = \left(\frac{\langle I_{det} \rangle}{\sigma_{det}} \right)^2 = \frac{\left(\sum_n \langle \tilde{I_n} \rangle \right)^2}{\sum_n \langle \tilde{I_n} \rangle^2}. \tag{16}$$

Note that changing $\Delta\lambda$ to a smaller step size and therefor increasing N will not change the result of $M_{spectral}$ as long as $\Delta\lambda$ is sufficiently small to sample the covariance μ_{mn}. The enabling property of the coherency matrix $\underline{J}$ is called *Toeplitz*, which implies an asymptotically behavior of its eigenvalues found by Grenander and Szegö (1958). Gray (2006) gives a simplified prove in Corollary 2.1 and 2.2 that both, numerator and denominator in Eq. (16) converge for large N.

4.3 Detector Averaging

In step $n = 3$ an averaging due to the integration of the instrument detector pixel takes place. We already established, that the resultant intensity distribution at the detector $I_{det}(a, b)$ is given by the summation in Eq. (12). This effect impacts the speckle contrast if individual speckles are not sufficiently oversampled by the instrument detector pixel grid $(\tilde{a}, \tilde{b})$. An analytical expression for the degrees of freedom $M_{detector}$ introduced by stationary speckles in one detector pixel with relative coordinates $(\Delta a, \Delta b)$ is given by

$$M_{detector} = \left[\frac{1}{A_D^2} \iint_{-\infty}^{\infty} K_D(\Delta a, \Delta b) \, |\mu_{det}(\Delta a, \Delta b)|^2 \, d\Delta a \, d\Delta b \right]^{-1}, \tag{17}$$

where A_D is the area of a detector pixel, $K_D(\Delta a, \Delta b)$ is the autocorrelation function of the detector pixel, and $\mu_{det}(\Delta a, \Delta b)$ is the field correlation at the detector plane (Goodman, 2007, p. 108). In order to accurately describe μ_{det} one needs to account for the evolution of the speckle size during the summation in Eq. (12). Let us consider a single speckle correlation area $I_1(S_d/2 \leq |x_1|, S_d/2 \leq |y_1|, f_1)$ with a spatial extend denoted by S_d centered at (x_1, y_1) in the slit. Its correlation relative to this position is described by

$$\Psi(\Delta x, \Delta y) = \frac{\int_{\infty}^{\infty} |P(g,h)|^2 \, e^{-i\frac{2\pi}{\lambda z}(g\Delta x + h\Delta y)} dg \, dh}{\int_{\infty}^{\infty} |P(g,h)|^2 \, dg \, dh}, \tag{18}$$

https://doi.org/10.5194/amt-2020-343
Preprint. Discussion started: 9 September 2020


Atmospheric Measurement Techniques Discussions

with $\Delta x = x - x_1$ and $\Delta y = y - y_1$ being relative coordinates. The function $F_l(\Delta f)$ introduced previously, characterizes how the correlation area develops after n frequency steps at the same position, $I_n(S_d/2 \leq |x_1|, S_d/2 \leq |y_1|, f_n)$ with $n > 1$. In other words, it denotes the amount of spectral steps after which a single speckle seizes to exist at a fixed position. The initial position of the speckle at the detector is $(a_1, b_1) = (M_x x_1, M_y y_1 + k\frac{c}{f_1})$. The subsequent contributions relative to the initial position are shifted by $k(\frac{c}{f_1} - \frac{c}{f_n})$ and have a magnitude denoted by $F_l(f_1 - f_n)$. Therefore, the resultant speckle correlation function at the detector $\mu_{det}(\Delta a, \Delta b)$ is a convolution of $|\Psi(\Delta a, \Delta b(\Delta f))|^2$ with $|F_l(\Delta f)|^2$.

4.4 Predicted SFA

The predicted reduced speckle contrast at the instrument detector plane using Eq. (7) corresponds to the SFA and is

$$SFA = C_{reduced} = \frac{1}{\sqrt{M_{polarization} M_{spectral} M_{detector}}}. \tag{19}$$

5 Results and Discussion

In the following we present and compare the SFA results from the measurement chain of Sect. 3 with the ones from the prediction model of Sect. 4 in the NIR and SWIR regime. The values of relevant parameters used are depicted in Table 1. They were chosen to represent a proposed instrument for ESA's CO2M mission (Meijer et al. (2019)).

By calculating the frequency correlation of subsequent monochromatic speckle images $I(x, y, \frac{c}{f_n})$ the fitted mean free path length of our diffuser sample is determined as $l_s = 53\mu\mathrm{m}$, which is close to the manufactures' specification of $55\mu\mathrm{m}$. This value may also reflect small instabilities of the speckle stationarity in the slit plane, which induce a smaller correlation between subsequent speckle intensities and therefore a shorter effective mean free path length. Table 2 shows the SFA values of the measurements and predictions with their corresponding intermediate averaging factors $M_{polarization}$, $M_{spectral}$, and $M_{detector}$ introduced in Sect. 4. Their counterparts from the measurement are deducted by calculating the speckle contrast at intermediate steps in the measurement chain. To verify the factor $M_{polarization} = 2$ a linear polarizer is placed *after* the diffuser and the measured speckle contrast compared to the nominal case rises by a factor of $\sqrt{2}$. Additionally, the polarization axis is rotated to different random positions without changing the result, which confirms the assumption made in Sect. 4, that the light exiting the diffuser is depolarized. With an ideal measurement chain the speckle contrast expected in the slit plane for monochromatic polarized speckles is $C_{slit,ideal} = 1$. This is the numerator in Eq. (19). The measured contrast in the slit is smaller, probably due to detector noise as suggested by Postnov et al. (2019). Webster et al. (2003) attributed the reduced measured contrast straylight from multiple reflections in their setup. The experimental factors $M_{spectral,measured}$ and $M_{detector,measured}$ are calculated in similar way using the relations,

$$C_{spectral,measured} = \frac{\langle C_{slit,measured} \rangle}{\sqrt{M_{spectral,measured}}}, \tag{20}$$

$$C_{detector,measured} = \frac{\langle C_{spectral,measured} \rangle}{\sqrt{M_{detector,measured}}}. \tag{21}$$

The results show a good agreement of prediction model and measurement. For the NIR regime the measured spectral averaging $M_{spectral}$ is 7% higher, than predicted. We assume, that detector noise is averaged in this step, which will yield a higher

https://doi.org/10.5194/amt-2020-343
Preprint. Discussion started: 9 September 2020

Atmospheric Measurement Techniques Discussions

Table 1. Sample spectrometer parameters used for the measurement and prediction. They were chosen to represent a proposed instrument for ESA's CO2M mission (Meijer et al. (2019)).

parameter	Value
M_x	0.34
M_y	0.30
aperture diameter	40.0mm
slit dimensions (x, y-direction)	295, 152µm
detector dimensions(a, b-direction)	105, 45µm
telescope focal length	131mm
d	3 mm
l_s	53 µm
NIR specific	
λ_{res}	0.12 nm
$\lambda_1 ... \lambda_N$	776.0 nm - 777.8 nm
n_s	1.454
$\Delta\lambda$	1 pm
SWIR specific	
λ_{res}	0.4 nm
$\lambda_1 ... \lambda_N$	1571 nm - 1573.5 nm
n_s	1.444
$\Delta\lambda$	2.5 pm

Type	$M_{polarization}$	$M_{spectral}$	$M_{detector}$	SFA
Measurement NIR	2	59	548	0.0040
Prediction NIR	2	55	536	0.0041
Measurement SWIR	2	31	192	0.0092
Prediction SWIR	2	30	191	0.0093

Table 2. Comparison SFA results of the measurement chain with the prediction model.

effective averaging factor. The SWIR measurement spectral averaging factor shows a smaller deviation of 2%, which we also attribute to averaged detector noise. The measured detector averaging factor $M_{detector}$ for both wavelength regimes indicates no correlation of features between adjacent instrument detector pixel due to its high value (Goodman, 2007, p. 109). It is also dependent on detector noise, which explains the slightly higher averaging factors than predicted.

https://doi.org/10.5194/amt-2020-343
Preprint. Discussion started: 9 September 2020

Atmospheric Measurement Techniques Discussions

6 Conclusions

We demonstrated a comprehensive and numerical approach to quantify diffuser induced spectral features during solar calibration of space imaging spectrometers, which is based on established speckle theory concepts. We compared our prediction results with a current measuring method and observed a good agreement. The presented speckle averaging mechanisms are not a complete representation of the real in-orbit situation of an instrument. The effect of the Sun's disk, which consists of many incoherent points sources distributed over a 0.5 degree angle, needs to be taken into account as well as the averaging due to the movement of the instrument relative to the Sun. Also, unlike the used laser point sources for the measurements, the Sun's light features an additional orthogonal polarization state, adding two polarization configurations to $M_{polarization}$ in the case of a highly scattering volume diffuser. The presented approach can be used for other diffuser types and optical geometries as well. It provides a solid starting point for future investigations into angular averaging mechanisms, which will complement the description of speckle reduction effects in imaging spectrometers of this type.

Data availability. The datasets generated and/or analyzed for this work are available from the corresponding author on reasonable request, subject to confirmation of Airbus Defence and Space GmbH.

Author contributions. Florian Richter was responsible for the acquisition and the analysis of the measurement data supported by all co-authors. Florian Richter developed the prediction model supported by Jerome Caron with insights about polarization contributions and properties of coherency matrices and revised by Corneli Keim and Mark Wenig. Florian Richter prepared the manuscript with contributions and critical revision from all co-authors.

Competing interests. The authors declare, that they have no conflict of interest.

Acknowledgements. The fused silica diffuser HOD®-500 used in this work was provided by Frank Nürnberg and Bernhard Franz, Heraeus Conamic, Germany.

https://doi.org/10.5194/amt-2020-343
Preprint. Discussion started: 9 September 2020

Atmospheric Measurement Techniques Discussions

References

Ahlers, B., Courreges-Lacoste, G. B., Schrijvers, C., and van Brug, H.: In-orbit detection of spectral features in SCIAMACHY, in: Sensors, Systems, and Next-Generation Satellites VIII, edited by Meynart, R., Neeck, S. P., and Shimoda, H., SPIE, https://doi.org/10.1117/12.565565, 2004.

Bevan, A.: Statistical Data Analysis for the Physical Sciences, Cambridge University Press, https://doi.org/10.1017/cbo9781139342810, 2009.

Burns, T., Ferreria, L., Keim, C., Prieto, L. P., Krauser, J. S., and Weise, D.: Sentinel-5: a novel measurement approach to quantify diffuser induced spectral features, in: International Conference on Space Optics — ICSO 2016, edited by Karafolas, N., Cugny, B., and Sodnik, Z., SPIE, https://doi.org/10.1117/12.2296079, 2017.

Clermont, L., Mazy, E., Marquet, B., and Plesseria, J.-Y.: An in-flight calibration assembly for the earth observation instrument Sentinel-4 UVN, in: Astronomical Optics: Design, Manufacture, and Test of Space and Ground Systems II, edited by Hallibert, P., Hull, T. B., and Kim, D. W., SPIE, https://doi.org/10.1117/12.2529572, 2019.

Dainty, J. C., Ennos, A. E., Françon, M., Goodman, J. W., McKechnie, T. S., and Parry, G.: Laser Speckle and Related Phenomena, Springer Berlin Heidelberg, https://doi.org/10.1007/bfb0111434, 1975.

Fletcher, K., Rider, H., and Agency, E. S.: Report for Mission Selection: Carbonsat Flex, ESA SP, ESA Communication Production Office, https://books.google.de/books?id=nkyrDAEACAAJ, 2015.

Goodman, J. W.: Speckle Phenomena in Optics: Theory and Application, Roberts & Company Publishers, 2007.

Gray, R. M.: Toeplitz and Circulant Matrices: A review, 2006.

Grenander, U. and Szegö, G.: Toeplitz Forms and their Applications, University of California Press, 1958.

Guehne, T., Keim, C., Bartsch, P., Weiss, S., Melf, M., and Seefelder, W.: Sentinel-5 instrument: status of design, performance, and development, in: Sensors, Systems, and Next-Generation Satellites XXI, SPIE, https://doi.org/10.1117/12.2278564, 2017.

Lorenzo, J. R.: Principles of Diffuse Light Propagation, World Scientific Publishing Company, https://www.ebook.de/de/product/11434141/jorge_ripoll_lorenzo_principles_of_diffuse_light_propagation.html, 2012.

Martimort, P., Fernandez, V., Kirschner, V., Isola, C., and Meygret, A.: Sentinel-2 MultiSpectral imager (MSI) and calibration/validation, in: 2012 IEEE International Geoscience and Remote Sensing Symposium, IEEE, https://doi.org/10.1109/igarss.2012.6351960, 2012.

Meijer, Y., Boesch, H., Bombelli, A., Brunner, D., Buchwitz, M., Ciais, P., Crisp, D., Engelen, R., Holmlund, K., Houweling, S., Janssens-Meanhout, G., Marshall, J., Nakajima, M., B.Pinty, Scholze, M., Bezy, J.-L., Drinkwater, M., Fehr, T., Fernandez, V., Loescher, A., Nett, H., and Sierk, B.: Coernicus CO2 Monitoring Mission Requirements Document, techreport 2, European Space Agency, Earth and Mission Science Division, 2019.

Nieke, J. and Mavrocordatos, C.: Sentinel-3a: commissioning phase results of its optical payload, in: International Conference on Space Optics — ICSO 2016, edited by Karafolas, N., Cugny, B., and Sodnik, Z., SPIE, https://doi.org/10.1117/12.2296174, 2017.

Olij, C., Schaarsberg, J. G., Werij, H. G., Zoutman, E., Baudin, G., Chommeloux, B., Bezy, J.-L., and Gourmelon, G.: Spectralon diffuser calibration for MERIS, in: Sensors, Systems, and Next-Generation Satellites, edited by Fujisada, H., SPIE, https://doi.org/10.1117/12.298122, 1997.

Postnov, D. D., Cheng, X., Erdener, S. E., and Boas, D. A.: Choosing a laser for laser speckle contrast imaging, Scientific Reports, 9, https://doi.org/10.1038/s41598-019-39137-x, 2019.

https://doi.org/10.5194/amt-2020-343
Preprint. Discussion started: 9 September 2020

Richter, A., Wittrock, F., Ladstaetter-Weissenmayer, A., and Burrows, J.: Gome measurements of stratospheric and tropospheric BrO, Advances in Space Research, 29, 1667–1672, https://doi.org/10.1016/s0273-1177(02)00123-0, 2002.

Richter, F., Krauser, J. S., Keim, C., Weise, D., and Wenig, M.: A novel measurement approach to quantify diffuser induced Spectral Features, in: Sensors, Systems, and Next-Generation Satellites XXII, edited by Neeck, S. P., Kimura, T., and Martimort, P., SPIE, https://doi.org/10.1117/12.2501943, 2018.

Thompson, C. A., Webb, K. J., and Weiner, A. M.: Imaging in scattering media by use of laser speckle, Journal of the Optical Society of America A, 14, 2269, https://doi.org/10.1364/josaa.14.002269, 1997a.

Thompson, C. A., Webb, K. J., and Weiner, A. M.: Diffusive media characterization with laser speckle, Applied Optics, 36, 3726, https://doi.org/10.1364/ao.36.003726, 1997b.

van Brug, H. and Courrèges-Lacoste, G. B.: Spectral features, effects, and cures, in: Earth Observing Systems XII, edited by Butler, J. J. and Xiong, J., SPIE, https://doi.org/10.1117/12.731012, 2007.

van Brug, H. and Scalia, P. S.: New approach to spectral features modeling, in: Earth Observing Systems XVII, edited by Butler, J. J., Xiong, X., and Gu, X., SPIE, https://doi.org/10.1117/12.931497, 2012.

van Brug, H. H., Vink, R., Schaarsberg, J. G., Courreges-Lacoste, G. B., and Snijders, B.: Speckles and their effects in spectrometers due to on-board diffusers, in: Earth Observing Systems IX, edited by Barnes, W. L. and Butler, J. J., SPIE, https://doi.org/10.1117/12.559596, 2004.

Webster, M. A., Webb, K. J., Weiner, A. M., Xu, J., and Cao, H.: Temporal response of a random medium from speckle intensity frequency correlations, Journal of the Optical Society of America A, 20, 2057, https://doi.org/10.1364/josaa.20.002057, 2003.

Wenig, M., Kuehl, S., Beirle, S., Bucsela, E., Jaehne, B., Platt, U., Gleason, J., and Wagner, T.: Retrieval and analysis of stratospheric NO2 from the Global Ozone Monitoring Experiment, Journal of Geophysical Research: Atmospheres, 109, n/a–n/a, https://doi.org/10.1029/2003jd003652, 2004.